



Impact of East Asian summer monsoon on the air quality over China: View from space

Chun Zhao,^{1,2} Yuhang Wang,¹ Qing Yang,¹ Rong Fu,³ Derek Cunnold,^{1,5} and Yunsoo Choi⁴

Received 27 June 2009; revised 23 September 2009; accepted 23 November 2009; published 4 May 2010.

[1] Tropospheric O₃ columns retrieved from Ozone Monitoring Instrument and Microwave Limb Sounder measurements, CO columns retrieved from Measurements of Pollution in the Troposphere, and tropospheric O₃ and CO concentrations retrieved from the Tropospheric Emission Spectrometer from May to August in 2006 are analyzed using the Regional Chemical and Transport Model to investigate the impact of the East Asian summer monsoon on the air quality over China. The observed and simulated migrations of O₃ and CO are in good agreement, demonstrating that the summer monsoon significantly affects the air quality over southeastern China, and this influence extends to central East China from June to July. Enhancements of CO and O₃ over southeastern China disappear after the onset of the summer monsoon and reemerge in August after the monsoon wanes. The premonsoon high O₃ concentrations over southern China are due to photochemical production from pollutant emissions and the O₃ transport from the stratosphere. In the summer monsoon season, the O₃ concentrations are relatively low over monsoon-affected regions because of the transport of marine air masses and weak photochemical activity. We find that the monsoon system strongly modulates the pollution problem over a large portion of East China in summer, depending on its strength and tempo-spatial extension. Model results also suggest that transport from the stratosphere and long-range transport from East China and South/central Asia all make significant contributions to O₃ enhancements over West China. Satellite observations provide valuable information for investigating the monsoon impact on air quality, particularly for the regions with limited in situ measurements.

Citation: Zhao, C., Y. Wang, Q. Yang, R. Fu, D. Cunnold, and Y. Choi (2010), Impact of East Asian summer monsoon on the air quality over China: View from space, *J. Geophys. Res.*, 115, D09301, doi:10.1029/2009JD012745.

1. Introduction

[2] During the past two decades, the rapid economic growth in China resulted in a significant increase in pollutant emissions [*Streets and Waldhoff*, 2000; *Streets et al.*, 2003; *Richter et al.*, 2005]. These emissions lead to the formation of elevated concentrations of pollutants (e.g., O₃ and CO) near the surface, mostly over East China [e.g., *Wei et al.*, 1999; *Ma et al.*, 2002; *H. Wang et al.*, 2006; *Zhao and Wang*, 2009]. The problem is worsened by the “basin” feature of three connected plains in this region with mountains to the west and

the ocean to the east; this region with a concentrated pollutant source also hosts a major portion of the Chinese population [*Zhao et al.*, 2009a]. Pollutant distributions are strongly affected by atmospheric circulations. Over China, the East Asian summer monsoon is a major atmospheric system affecting air mass transport, convection, and precipitation [*Hoskins and Rodwell*, 1995; *Rodwell and Hoskins*, 2001; *Ding and Chan*, 2005].

[3] Limited available surface observations show that near-surface O₃ concentrations can be strongly perturbed by the monsoonal flow with clean oceanic air masses transported from the tropical Pacific Ocean in summer [e.g., *Tanimoto et al.*, 2005; *Z. Wang et al.*, 2006; *Li et al.*, 2007; *He et al.*, 2008]. *Tanimoto et al.* [2005] analyzed the surface O₃ seasonality observed at the Acid Deposition Monitoring Network in East Asia sites, and *Li et al.* [2007] analyzed observations at three mountain sites in central East China. Both found a late spring/early summer maximum followed by a summer minimum in surface O₃ concentrations over East China. The rapid decrease in surface O₃ in the May–June period in southern China results from the onset of the East Asian monsoon over the region.

¹School of Earth and Atmospheric Sciences, Georgia Institute of Technology, Atlanta, Georgia, USA.

²Now at Atmospheric Sciences and Global Change Division, Pacific Northwest National Laboratory, Richland, Washington, USA.

³Jackson School of Geosciences, The University of Texas at Austin, Austin, Texas, USA.

⁴Jet Propulsion Laboratory, California Institute of Technology, Pasadena, California, USA.

⁵Deceased 18 April 2009.

[4] In contrast to East China, surface O₃ observations at Mount Waliguan (WLG) (36.3°N, 100.5°E) station, located in a remote region on the northeastern boundary of the Qinghai-Tibetan plateau over West China, show a clear summer maximum [e.g., *Zhu et al.*, 2004; *T. Wang et al.*, 2006]. Several mechanisms were proposed. *Zhu et al.* [2004] analyzed the surface O₃ measurements at the WLG station with a 3-D chemical transport model and concluded that high O₃ in summer over West China is due to monsoonal transport from East China and long-range transport from South/central Asia and even Europe. On the other hand, analysis of back trajectories and surface measurements of O₃, CO, and NO_y by *T. Wang et al.* [2006] and *Ding and Wang* [2006] suggested that downward transport of upper tropospheric and stratospheric air masses is the main contributor to high summer O₃ over West China.

[5] A number of studies using recently available satellite measurements examined the impact of Asian monsoon systems (including East Asian monsoon and India monsoon) on the tropospheric composition, particularly in the upper troposphere [e.g., *Randel and Park*, 2006; *Fu et al.*, 2006; *Jiang et al.*, 2007; *Park et al.*, 2007; *Worden et al.*, 2009]. *Randel and Park* [2006] found that the convection associated with the Asian monsoon transports air masses of low O₃ and high water vapor from the marine boundary layer into the upper troposphere based on Aura Atmospheric Infrared Sounder data. *Jiang et al.* [2007] showed that deep convection associated with the Asian monsoon lifts the boundary layer air masses with high CO concentrations into the upper troposphere through analysis of the Aura Microwave Limb Sounder (MLS) data. Using Tropospheric Emission Spectrometer (TES) observations, *Worden et al.* [2009] found O₃ enhancement in June and July and O₃ decrease in August, in the upper troposphere (~300 hPa) over central and South Asia, corresponding to the onset and dissipation of the Indian monsoon.

[6] Publicly available in situ observations provide insufficient spatial coverage to resolve the spatially temporal progress of the East Asian monsoon impact on the air quality over China. The measurement gaps can be mitigated by available satellite observations. Previous studies tend to focus on either the lower tropospheric impact at selected locations where in situ observations are available or the upper tropospheric impact using satellite observations. Several recent studies have shown that satellite instruments based on thermal-infrared observations (e.g., Measurements of Pollution in the Troposphere (MOPITT) and TES) are generally sensitive to trace gases in the lower troposphere [e.g., *Deeter et al.*, 2007; *Clerbaux et al.*, 2008; *Kar et al.*, 2008; *Shim et al.*, 2009; *Halland et al.*, 2009]. *Deeter et al.* [2007] found that the retrieval sensitivity of MOPITT to lower tropospheric CO is significant over the continent during daytime. *Shim et al.* [2009] examined the lower tropospheric pollution outflow of Mexico City using TES measurements.

[7] In this study, we attempted to combine satellite observations throughout the troposphere with model simulations using a 3-D regional chemical transport model (Regional Chemical and Transport Model (REAM)) to provide a holistic view of the monsoon impact on tropospheric pollutant distributions over China. Here we refer the term “air quality” to pollutant distributions in the troposphere, although we place an emphasis on the lower troposphere in the

modeling analysis. We apply multiplatform satellite observations by the MOPITT instrument onboard the NASA Terra satellite, the Ozone Monitoring Instrument (OMI), the MLS, and the TES onboard the NASA Aura satellite. We will show the potential of using the current generation of satellite instruments to monitor air quality changes caused by the monsoon circulation. REAM will also be used to simulate the monsoon impact and assess the source contributions to regional O₃ by chemical production from anthropogenic NO_x emitted over China, transport from the stratosphere, and long-range transport from South/central Asia.

[8] In section 2 and 3, we describe the satellite measurements and the REAM model used in the study. The observed and simulated variations of tropospheric CO and O₃ distributions and their relationships to monsoon circulation over China in the summer of 2006 are investigated in section 4. Conclusions are given in section 5.

2. Satellite Measurements

2.1. Global Precipitation Climatology Project (GPCP) One-Degree Daily Precipitation Data Set

[9] The One-Degree Daily (1DD) precipitation data are available from the GPCP Global Merge Development Center in the NASA/Goddard Space Flight Center Laboratory for Atmospheres. The data are estimated at a 1° daily resolution from multisatellite observations [*Huffman et al.*, 2001]. The current data set extends from October 1996 to the present. The primary product in the 1DD data set is a combined observation-only data set.

2.2. MOPITT Tropospheric CO Columns

[10] The MOPITT instrument onboard the NASA Terra satellite provides global CO observations. The satellite passes over the equator at around 1045 and 2245 LT, and the horizontal resolution of MOPITT is 22 km² × 22 km². Since the purpose of this study is to investigate the pollutant changes before, during, and after the monsoon season, the analysis is less sensitive to the systematic instrument biases. The measurements at nighttime are excluded in this study because the nighttime observations over land typically exhibit poor sensitivity to lower tropospheric CO [*Deeter et al.*, 2007]. Although a general positive bias of 20% of MOPITT CO columns in 2006 was found via the comparison to in situ measurements, a much smaller bias (~2%) occurred over major urban centers such as East China and Japan [*Emmons et al.*, 2009], where MOPITT CO measurements are used in the study. When compared with the MOPITT measurements, REAM results are processed with the MOPITT observation operator, also known as “averaging kernels” [*Deeter et al.*, 2003].

2.3. TES CO and O₃

[11] The TES instrument onboard the NASA Aura satellite passes over the equator at 1345 LT [*Beer et al.*, 2001]. The nadir horizontal resolution of TES is 5 km² × 8 km². TES CO and O₃ data are obtained from the NASA Langley Atmospheric Science Data Center. This analysis uses TES data taken during summer 2006 in global survey mode with a sampling of one observation every 160 km with 16 orbits per day; it takes 16 days to return to the same target location [*Beer*, 2006]. The estimated uncertainties of individual TES

CO and O₃ retrievals provided in the TES products are ~12 and ~15 ppbv, respectively. For O₃, only those data for which the degrees of freedom of signal for the lower troposphere below 600 hPa is 0.2 or larger are selected to ensure that the estimate is sensitive to the lower tropospheric O₃. Furthermore, the O₃ data with “C curve” shape are screened as discussed by *Worden et al.* [2009]. When compared with the TES measurements, the REAM results are processed with the TES observation operator for CO and O₃, respectively, to account for the different sensitivities and a priori information of TES retrievals to different pressure levels [*Jones et al.*, 2003]. The resulting model profiles can then be directly compared with TES retrievals without bias associated with the TES a priori information and vertical resolution [*Zhang et al.*, 2006; *Jourdain et al.*, 2007; *Worden et al.*, 2007].

2.4. OMI-MLS Tropospheric O₃ Columns

[12] The OMI and MLS instruments fly onboard the NASA Aura satellite, which passes over the equator at 1345 LT. The nadir horizontal resolution of OMI is 13 km² × 24 km². MLS is a limb-viewing instrument, and a single profile in standard products of MLS ozone measurements has a spatial resolution of 6 km cross-track and approximately 200 km along track [*Yang et al.*, 2007]. The tropospheric O₃ columns are derived using a residual method by estimating the stratospheric O₃ columns using MLS O₃ profiles above 215 hPa and subtracting that amount from OMI level 2 total column O₃ [*Yang et al.*, 2007]. The midlatitude stratospheric O₃ columns between 215 hPa and the tropopause are obtained by SAGE II mapping; the altitudes of the tropopause are taken from the National Centers for Environmental Prediction (NCEP) reanalysis data [*Yang et al.*, 2007]. The coincidence criteria for MLS stratospheric columns with OMI total column measurements are 1.25° × 1.25° on the same day. The tropospheric O₃ columns are derived in cloud-free condition, defined as cloud reflectivity of <30% based on the OMI 360 nm reflectivity data provided in the level 2 data sets. The OMI-MLS tropospheric O₃ columns are validated against ozonesonde measurements from the Intercontinental Chemical Transport Experiment (INTEX) Ozonesonde Network Study campaign in spring and summer over North America in 2006. Based on the comparisons against ozonesonde, the uncertainty of the individual derived OMI-MLS column is ~13% in summer. The detailed validation of the OMI-MLS tropospheric column O₃ products was described by *Yang et al.* [2007, 2009].

3. Model Description

[13] REAM driven by MM5 assimilated meteorological fields was described by *Choi et al.* [2008a]. In this work, we use REAM that is driven by Weather Research and Forecasting (WRF) -assimilated meteorological fields based on the NCEP reanalysis data [*Zhao et al.*, 2009b]. Previously, this model was applied to investigate a number of tropospheric chemistry and transport problems at northern mid-latitudes [*Choi et al.*, 2005, 2008a, 2008b; *Jing et al.*, 2006; *Y. Wang et al.*, 2006; *Guillas et al.*, 2008; *Zhao and Wang*, 2009; *Zhao et al.*, 2009a] and in the polar regions [*Zeng et al.*, 2003, 2006; *Y. Wang et al.*, 2006, 2007]. REAM has a horizontal resolution of 70 km with 23 vertical layers below 10 hPa. The time steps for transport and chemistry are 5 min

and 1 h, respectively. Most meteorological inputs in REAM are updated every 30 min, except those related to convective transport, which are updated every 5 min. The horizontal domain of WRF has five extra grids beyond that of REAM on each side to minimize potential transport anomalies near the boundary. Initial and boundary conditions for chemical tracers in REAM are obtained from the global simulation for the same period using the GEOS-CHEM model (v7-03-06) with assimilated meteorology (GEOS-4) [*Bey et al.*, 2001]. For our analysis period, the lateral boundary CO columns from GEOS-CHEM simulations are lower than the MOPITT measurements (likely because of an underestimation of biomass burning emissions). The difference is much larger than the ~2% bias of MOPITT CO columns over East China and Japan estimated by *Emmons et al.* [2009]. The reason is unknown. We therefore scaled the lateral boundary results from GEOS-CHEM such that the resulting monthly mean CO columns at lateral boundaries are consistent with MOPITT observations. The lateral boundary correction significantly increases the outflow of CO over the North Pacific, but not the CO columns over East China.

[14] Biogenic emission algorithms and inventories are adapted from the GEOS-CHEM model. The lightning NO_x emission is parameterized as done by *Zhao et al.* [2009b], although the model estimated effect is small as found by *Zhao and Wang* [2009]. The anthropogenic emissions of tracers other than NO_x are taken from a recent bottom-up Asian emission inventory developed by *Zhang et al.* [2009] for the 2006 INTEX-B campaign. Anthropogenic NO_x emissions for 2006 are obtained by scaling the NO_x emissions derived for 2007 over East Asia with an 8% annual rate of increase in China [*Zhao and Wang*, 2009]. The anthropogenic NO_x emissions (the dominant source of NO_x emissions) are assumed to be constant during our simulations for summer 2006; the assumption is supported by OMI-observed NO₂ columns (not shown). The NO_x and CO emissions from biomass burning are obtained from the Global Fire Emissions Database, Version 2 (GFEDv2.1; Oak Ridge National Laboratory Distributed Active Archive Center, Oak Ridge, Tennessee; available at <http://daac.ornl.gov/>).

4. Result and Discussion

4.1. East Asian Summer Monsoon over East China

[15] To assess the monsoon impact on the air quality over East China, an examination of time and location of the East Asian summer monsoon onset is necessary. The monsoon index, based on atmospheric thermodynamics and dynamics, such as pressure, ocean-land temperature contrast, wind field, precipitation, and so on, has been widely used to quantify the monsoon extent and its variability over monsoon regions [e.g., *Li and Zeng*, 2002; *Huang*, 2004; *Zhang et al.*, 2004]. Following *Wang and Lin* [2002] and *Zhang et al.* [2004], we define the East Asian summer monsoon index in this study as follows: (1) a zonal (110°E–120°E for East China) vertical wind shear between the low-level (e.g., 850 hPa) southerlies ($Wind_{south} > 0$) and upper level (e.g., 300 hPa) northerlies ($Wind_{north} > 0$), and (2) a mean rainfall of >6 mm/d. Using this index, the monsoon onset is determined not only by rainfall, but also by the establishment of a monsoon-driven circulation that is characterized by a change in the zonal vertical wind shear. *Ding and Chan* [2005] categorized the

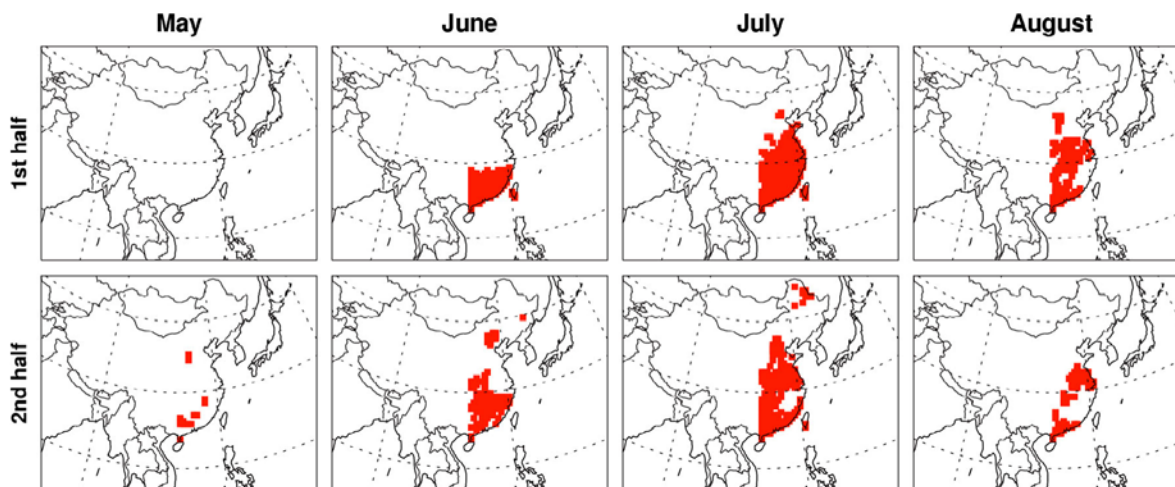


Figure 1. Progress of the East Asian summer monsoon onset over East China denoted by the monsoon indices (red squares) from May to August in 2006. The indices are calculated twice per month.

East Asian summer monsoon progress in several stages and showed that each stage has a time scale less than 1 month. Therefore, the index is defined on the basis of grid-by-grid calculations of wind shear and rainfall simulated by the WRF model averaged over a half-month period in this study.

[16] Figure 1 shows the half-monthly index of the East Asian summer monsoon over East China from May to August 2006. The red dots in the figure indicate the regions with an index equal to 1 (i.e., with monsoon onset); elsewhere the index is equal to 0. The spatial progress of the East Asian summer monsoon is very clear. The East Asian summer monsoon reaches south China in the second half of May and initiates the rainy season over southeastern and east central China in June. It advances northward up to northeastern China and covers the entire East China in July. The monsoon retreats back from northeast China in the first half of August and dissipates at the end of August. The progress of the East Asian summer monsoon in 2006 is generally consistent with the processes summarized by *Ding and Chan* [2005].

[17] The East Asian summer monsoon onset is always accompanied by heavy rainfall. Figure 2 shows GPCP-observed and WRF-simulated time-latitude cross sections of 5 day average daily precipitation over East China (110°E–120°E) from May to August in 2006. The heavy rainfall over southeast China commences in early May, which is not driven by the monsoon [*Zhang et al.*, 2004; *Ding and Chan*, 2005]. The monsoon-driven steep rise in precipitation starts from mid-May over southeast China. This rainy episode over southeast China continues into mid-June. Afterward, it rapidly shifts to east central China and lasts for ~20 days. On 5 July, the rainy season restarts over southeast China, with a time gap of 15 days between the first and this rainy episode as monsoon dynamics initiated in the tropics progresses northward [*Ding and Chan*, 2005]. By mid-July, the rain belt moves to northeast China, the northernmost position of the summer monsoon rainfall. This rainy season persists over northeast China for ~1 month. In mid-August, the rainy season ends. Afterward, most parts of East China are dominated by dry atmospheric circulations [*Ding and Chan*, 2005]. WRF successfully simulates the progress and distribution of the observed precipitation pattern with a correlation

coefficient of 0.72 and mean bias of 0.78 mm/d. The bias of WRF simulations has very limited effects on our analysis since we study the monsoon impact on regional and semi-monthly scales. During the rainy season, the photochemical process in the lower troposphere is significantly constrained (see section 4.3).

4.2. Impact of East Asian Summer Monsoon on Tropospheric CO over East China

[18] Figure 3 shows the monthly mean tropospheric CO columns retrieved from MOPITT and the corresponding model simulations from May to August in 2006. REAM successfully captures the variations of the tropospheric CO columns measured by MOPITT with a correlation coefficient of 0.7–0.75 and a mean bias within 10%. Both the measurements and model simulations indicate the high CO columns with an average of 2.3×10^{18} molecules/cm² over East China, Korea, Japan, and the North Pacific Ocean in May because of the CO emissions from the anthropogenic sources and the fires over Siberia. When the monsoon comes in and becomes dominant over southeast China in June (Figure 1), the enhancement of CO columns disappears over the region because of the monsoonal inflow of the oceanic air masses with lower CO concentrations. Following the northward migration of the monsoon (Figure 1), the CO columns over east central and northeast China are also significantly reduced in July (Figure 1). In June and July, the mean of CO columns over East China decrease by up to 35%. The high CO columns reemerge over East China in August when the monsoonal inflow dissipates (Figure 1).

[19] Figure 4 shows the comparison of TES-retrieved and model-simulated vertical distribution of CO mixing ratios from May to August in 2006 at 110°E–120°E and 20°N–40°N over East China. All data are interpolated to a 2° latitudinal band and a vertical interval of 100 hPa from 1000 to 300 hPa. The uncertainty of individual TES CO retrieval is estimated as ~12 ppbv obtained from the products. The use of monthly regional averages reduces the measurement uncertainty. While a thermal-infrared-based instrument such as TES may incur sensitivity changes, the data clearly show the difference between the northern region not affected by

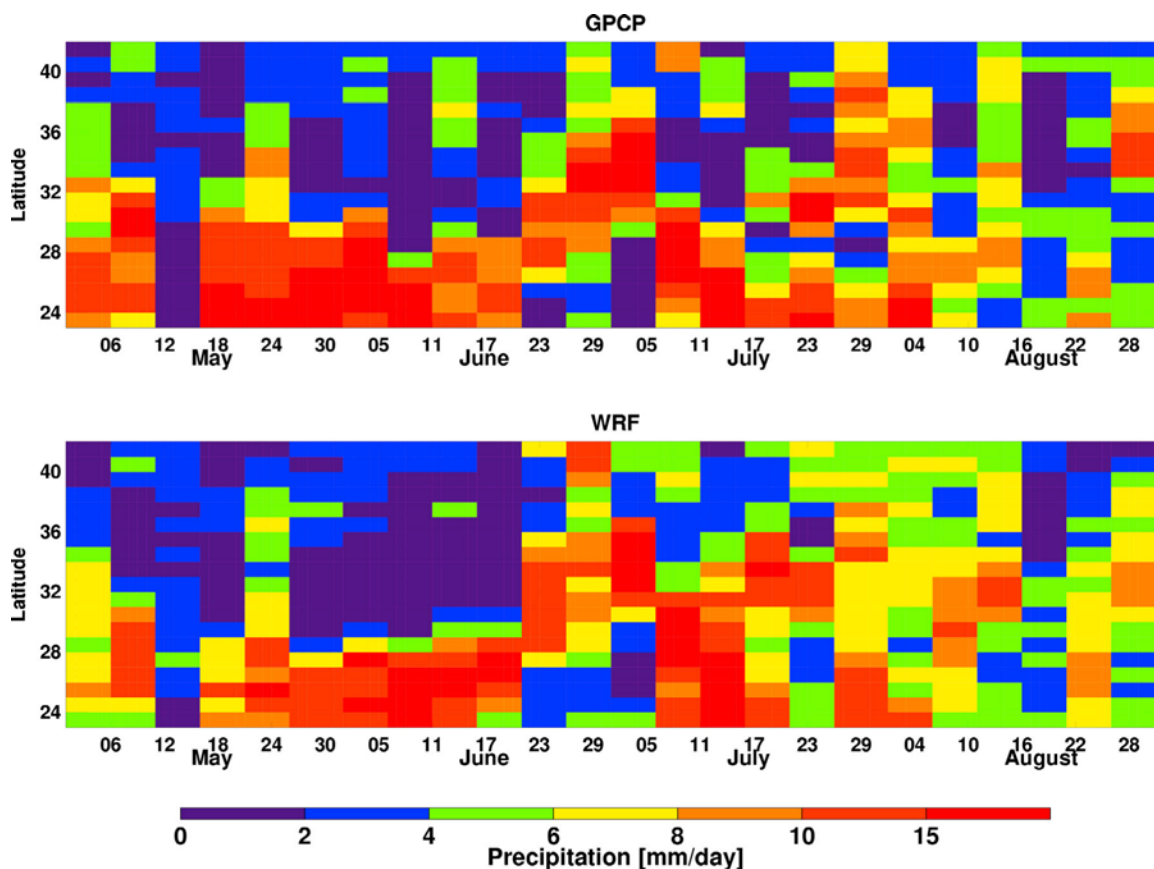


Figure 2. Time-latitude cross sections of GPCP satellite-observed and WRF-simulated 5 day average daily precipitation over East China (110°E – 120°E) from May to August in 2006.

monsoon and the southern region affected by monsoon. The distribution and temporal variation of TES CO concentrations from May to August are consistent with the MOPITT measurements (Figure 3). The simulated CO concentrations are also consistent with the measurements, but the mean is lower by up to $\sim 10\%$, probably from the underestimation of the anthropogenic CO emissions over China. The lower tropospheric CO concentrations decrease by $\sim 25\%$ from 160 ppbv in May to ~ 120 ppbv in June and July over southeast China and increase back to 140 ppbv in August. Two independent satellite products and the model simulations all point to the lower CO concentrations in June and July affected by the onset and progression of monsoon in the period. The gradient of CO concentrations between East China and the Pacific Ocean is larger in the lower troposphere than that in the free troposphere. Therefore, the monsoon inflow of clean marine air reduces the CO concentrations more significantly in the lower troposphere than in the free troposphere.

4.3. Impact of East Asian Summer Monsoon on Tropospheric O_3 over East China

[20] East Asian summer monsoon affects O_3 concentrations over East China by bringing in clean oceanic air masses and reducing photochemical production of O_3 in the lower troposphere related partly to clouds. Figure 5 shows the REAM-simulated time-latitude cross section of the 5 day average daytime O_3 production rate in the lower troposphere

(< 2 km) over East China (110°E – 120°E) from May to August in 2006. The reduction of O_3 production corresponds loosely to the increase in precipitation rates shown in Figure 2 with a correlation coefficient of -0.52 . Over southeastern China, the lower tropospheric photochemical O_3 production is significantly constrained by the presence of monsoon from May to mid-June. However, during the same period over eastern central and northeastern China, the lower tropospheric photochemical O_3 production rate is high, fostering a large amount of O_3 over the regions. The lower tropospheric O_3 production over eastern central and northeastern China becomes weaker in July and early August because of the northward advance of the monsoon. The lower tropospheric O_3 production revives to a higher rate over East China after mid-August when the monsoon dissipates.

[21] The reduction of the low tropospheric O_3 concentrations by the monsoon progress is shown in TES 825 hPa O_3 measurements. Figure 6 shows the time series of the monthly average O_3 concentrations over southeast (105°E – 120°E , 20°N – 30°N) and northeast (105°E – 120°E , 30°N – 40°N) China at 825 hPa from TES and the corresponding REAM simulations. There are at least 10 days of 25 measurements for each average over the region. The uncertainty of individual TES 825 hPa O_3 retrieval is estimated as ~ 15 ppbv obtained from the products. The use of monthly regional averages reduces the measurement uncertainty. The standard deviation of 825 hPa O_3 is 10–20 ppbv in this study. After averaging, the error of measurements is less than the standard

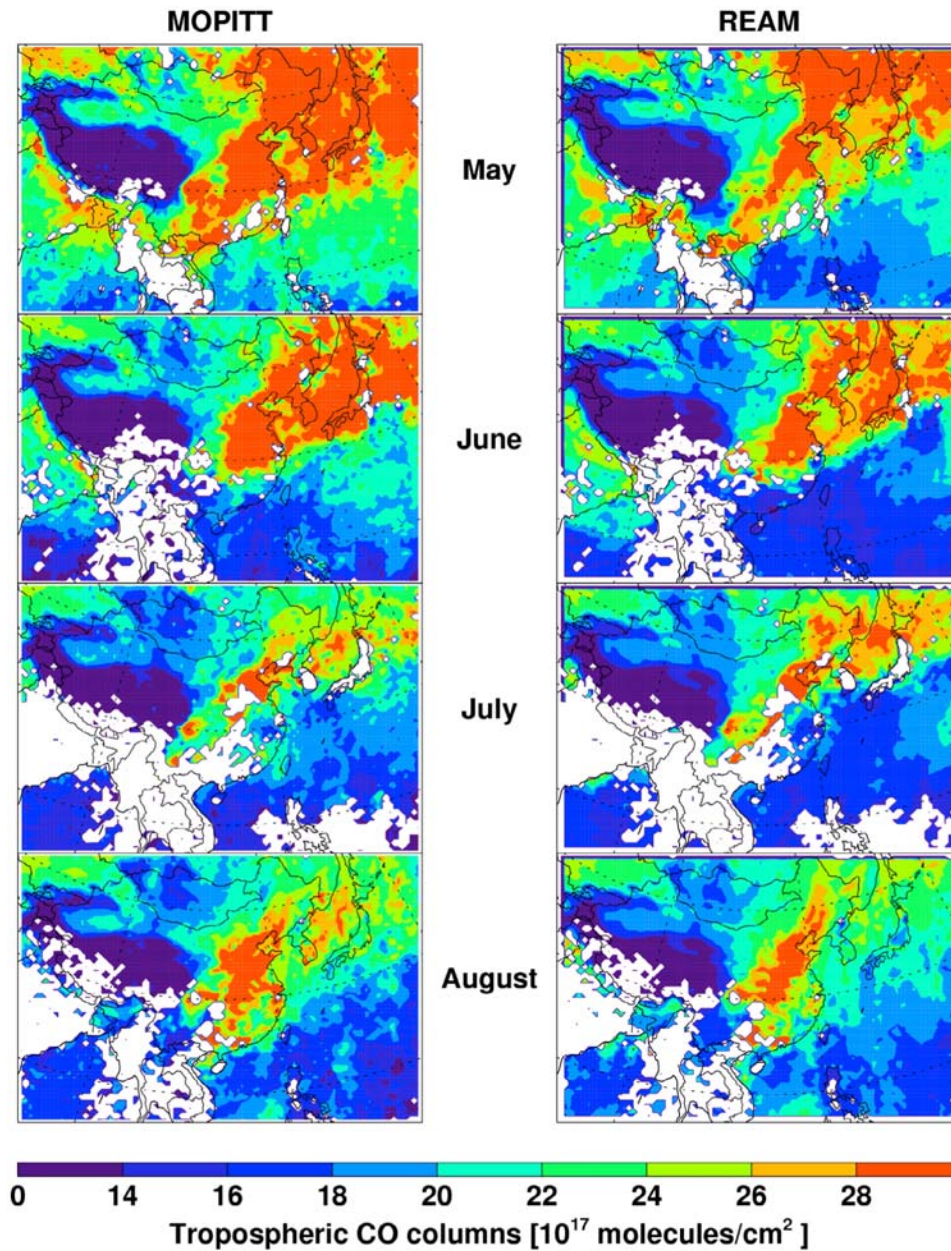


Figure 3. Monthly mean tropospheric CO columns retrieved from MOPITT and the corresponding REAM simulations from May to August in 2006. White areas denote no available MOPITT data. The model results have been processed with the MOPITT averaging kernel.

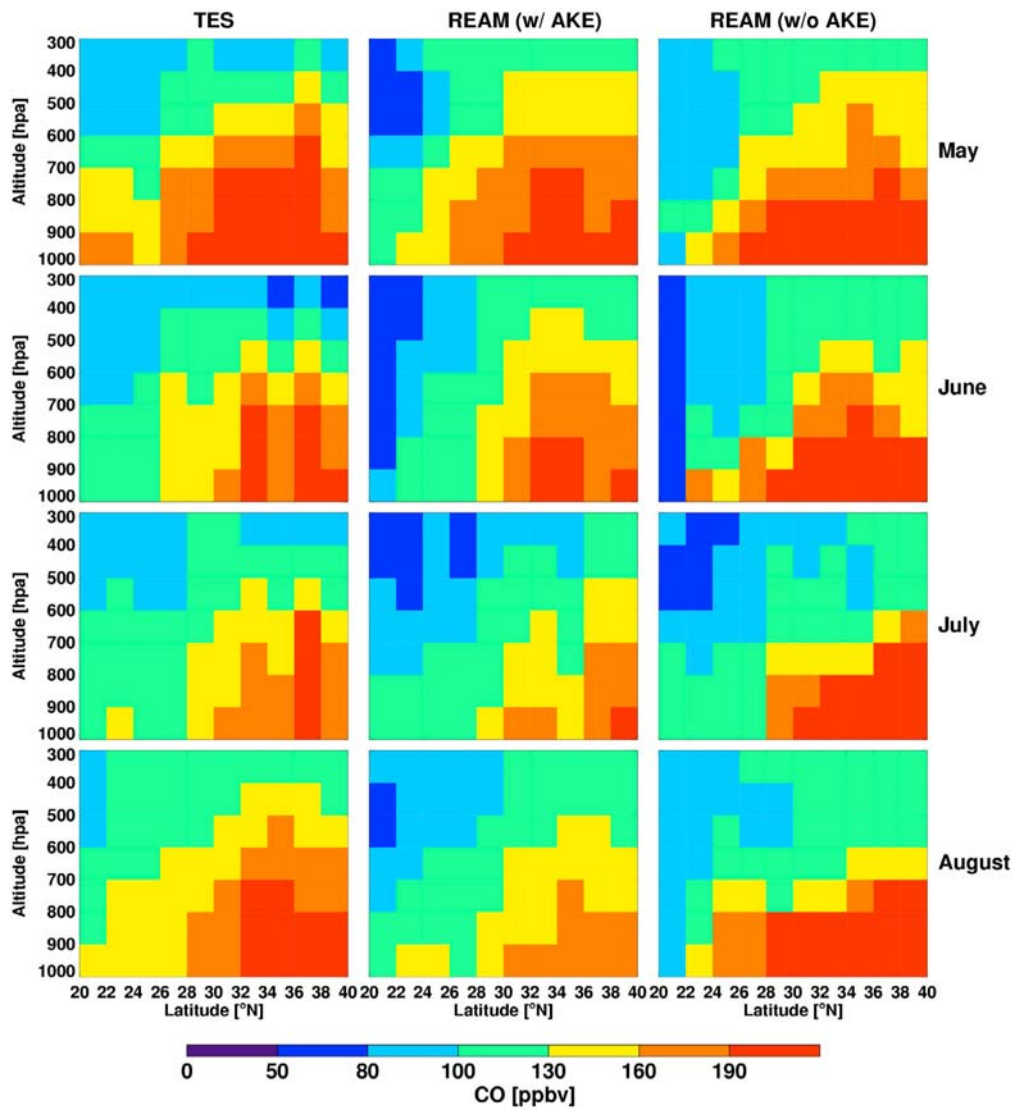


Figure 4. Latitude-altitude cross sections of TES-retrieved and REAM-simulated monthly mean CO concentration distributions from May to August in 2006 over East China (110°E–120°E) at 20°N–40°N from surface to 300 hPa. REAM (w/ AKE), model results processed with the TES CO averaging kernel; REAM (w/o AKE), original model results.

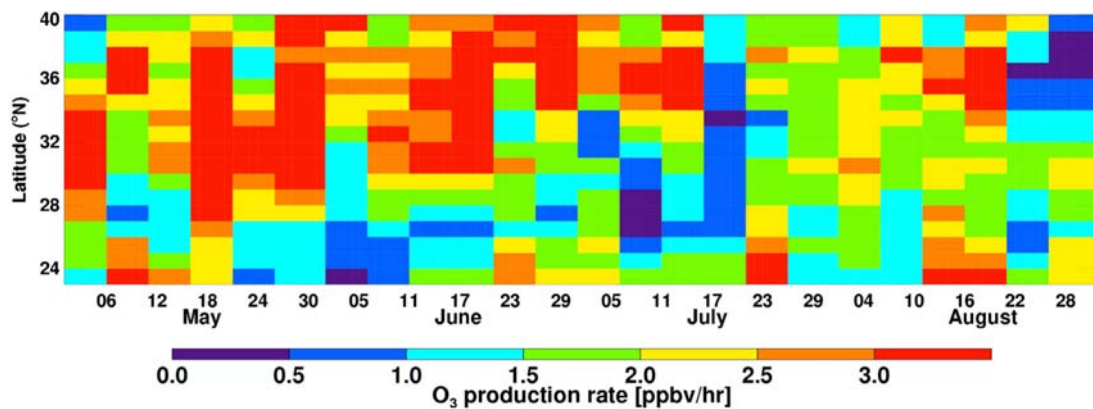


Figure 5. Time-latitude cross section of REAM-simulated 5 day average of daytime O₃ net production rate in the lower troposphere over East China (110°E–120°E) from May to August in 2006.

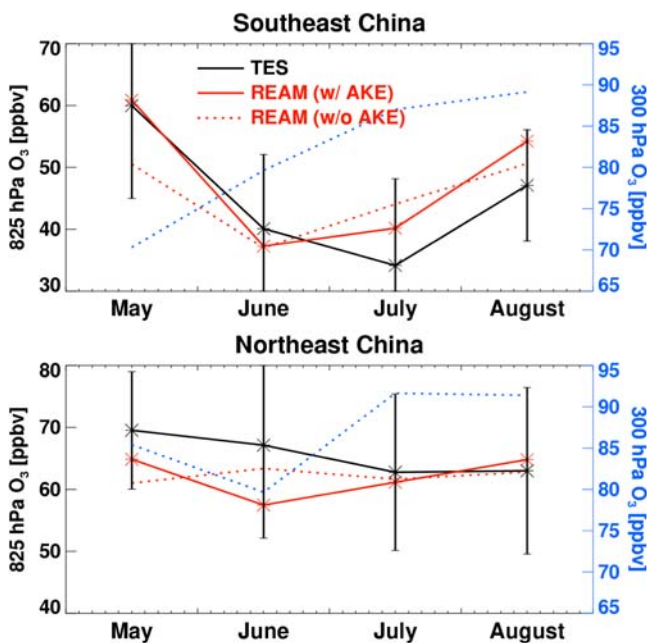


Figure 6. Time series of the monthly average O_3 concentrations over southeast and northeast China at 825 hPa from TES and the corresponding REAM simulations. Asterisks represent the observed and simulated means. The vertical bars represent the standard deviations of the observations. REAM (w/ AKE), model results processed with the TES O_3 averaging kernel; REAM (w/o AKE), original model results. The original modeled 300 hPa O_3 mixing ratios are also shown with blue dotted line.

deviation. So we used the standard deviation in the comparison. REAM generally captures the features of the measurements, and the biases are within the standard deviations of the measurements. Over southeast China, the TES-observed O_3 mixing ratio reaches up to 60 ppbv in late May, rapidly drops to 40 ppbv in June and July because of the monsoon impact, and increases back to 50 ppbv in August. The high O_3 concentrations in late May result from the recirculation of the large amounts of O_3 photochemically produced over east central and northeastern China (Figure 6) [Zhao *et al.*, 2009a]. The monsoon impact on lower tropospheric O_3 over southeast China is evident. Over northeast China, although the TES-observed average O_3 concentration is lower in July than in June and August, the summer monsoon impact is not as significant as that over southeast China. The standard deviation of the TES-measured O_3 is up to 20 ppbv, which can be attributed mostly to the uneven spatial distribution of the lower tropospheric O_3 . The simulated O_3 distribution shows the same pattern with minimum O_3 concentrations in June and July.

[22] Figures 7a and 7b show the half-monthly mean tropospheric O_3 columns derived from OMI-MLS measurements and the corresponding model simulations from May to August in 2006. The uncertainty of the individual OMI-MLS-derived tropospheric columns is $\sim 13\%$ in summer. The half-monthly average reduces the measurement uncertainty [Yang *et al.*, 2007]. The OMI-MLS O_3 columns indicate high tropospheric O_3 columns over entire East China from May to mid-June. The tropospheric O_3 enhancement is reduced over

southeast China after mid-June, and the reduction effect extends to northeast China in July. The tropospheric O_3 enhancement over East China reemerges around mid-August. REAM captures the general patterns of the observed tropospheric O_3 distributions over East Asia and the monsoon-driven O_3 variations. The correlation coefficient between the model simulations and measurements is 0.7–0.9, and the difference is within $\sim 10\%$.

[23] Three sensitivity simulations are conducted to understand the main contributors to the simulated tropospheric O_3 distributions. One is a simulation without anthropogenic NO_x emissions over East Asia. The second one is a simulation without the stratospheric contributions. To calculate the effect of the stratospheric O_3 transport, we use the same approach as Choi *et al.* [2008b], in which we run tagged tracer simulations using GEOS-CHEM to compute the fractions of O_3 transported from the stratosphere. We remove the stratospheric contribution in the REAM sensitivity simulation by using only the tropospheric portions of initial conditions and lateral and upper boundary conditions for O_3 . The third one is a simulation without the transport of anthropogenic O_3 from South/central Asia ($0^\circ N$ – $50^\circ N$, $60^\circ E$ – $90^\circ E$), in which the anthropogenic NO_x emissions over South/central Asia in the REAM and GEOS-CHEM simulations are turned off. The effects of these factors on tropospheric O_3 columns are estimated by comparing O_3 in the sensitivity simulations with the standard simulation. The results are shown in Figure 7 (the rightmost three columns).

[24] Photochemically produced tropospheric O_3 columns over East China, in particular northeast China, generally increase from May to August (Figures 7a and 7b, the third column). The constraint on the lower tropospheric photochemical O_3 production by the monsoon progress over East China is not apparent in terms of the tropospheric columns because the constrained photochemical O_3 production in the lower troposphere is compensated for by the enhanced O_3 production in the free troposphere (outflow regions), where the impact of precipitation and clouds is limited, which is shown by the simulated 300 hPa O_3 concentrations in Figure 6. Generally, 300 hPa O_3 concentrations increase from May to June and July, attributed primarily to increasing solar insolation and water vapor. The contribution from stratospheric transport to tropospheric O_3 columns over East China is the largest and comparable to photochemical production in May, and it decreases to the smallest in July and August. Transport of O_3 from the stratosphere over East China decreases from May to July and August as wave propagation from the troposphere to stratosphere weakens in summer [e.g., Wang *et al.*, 1998, and references therein]. Over East China, the impact of the O_3 transported from South/central Asia is much smaller than the former two contributors in May and June but comparable to, if not larger than, stratospheric transport in July and August. The South/central Asia O_3 is mostly transported via southwest China in May and June but via northwest China in July and August, because the transport is largely driven by India summer monsoon, which starts in May and June over South India and moves to North India and central Asia in July and August.

[25] The enhancement of tropospheric O_3 columns over East China from May to mid-June is attributed to the combination of the regional fast photochemical O_3 production and stratospheric O_3 transport. In July, the tropospheric O_3

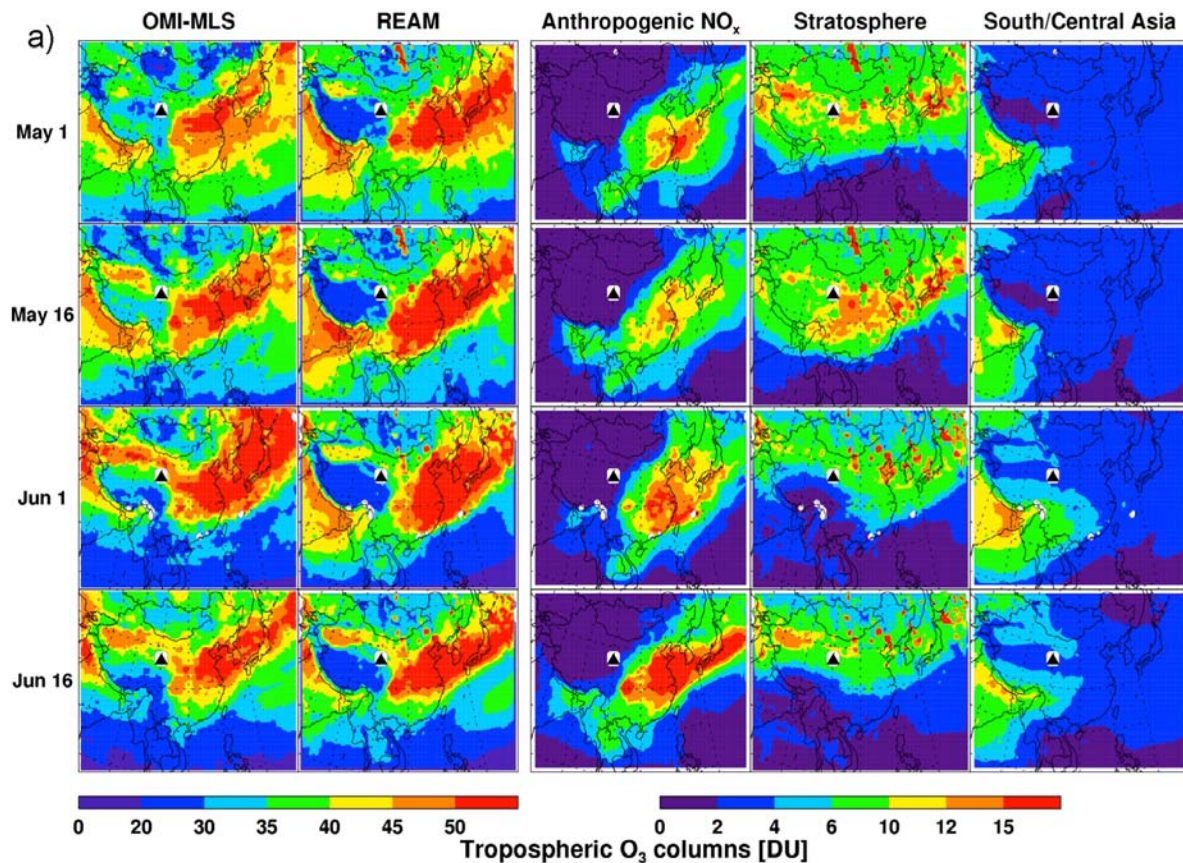


Figure 7. (a) Half-monthly mean tropospheric O_3 columns from May to June in 2006 derived from OMI-MLS satellite measurements (first column), REAM simulations (second column), O_3 produced from anthropogenic NO_x emissions over East Asia (third column), O_3 transported from the stratosphere (fourth column), and O_3 transported from South/central Asia (fifth column). The black triangle represents the location of the WLG station. (b) Same as Figure 7a but for July and August in 2006.

columns drop down to the minimum over East China because of the monsoonal inflow and the constrained photochemical process in the lower troposphere. The O_3 enhancement reemerges around mid-August because of the revived fast lower tropospheric photochemical production of O_3 along with the retreat of the monsoon. The monsoon impact on tropospheric O_3 is more significant over southeast China than over northeast China.

4.4. Summer Tropospheric O_3 Enhancement over West China

[26] Previously, *Zhu et al.* [2004] and *T. Wang et al.* [2006] found high O_3 concentrations over West China in late spring and summer based on the surface measurements at the WLG station over West China [e.g., *Zhu et al.*, 2004; *T. Wang et al.*, 2006]. The O_3 enhancements are attributed to different reasons by the two studies (see section 1). A band of tropospheric O_3 enhancement (40–50 DU) over West China (36°N–42°N, 80°E–100°E) is also observed by the OMI-MLS O_3 columns from May to August in 2006 (Figures 7a and 7b). The band of high tropospheric O_3 columns is mostly to the north of 35°N because of the presence of the Himalayas and the Tibetan Plateau south of 35°N [*Zhu et al.*, 2004]. REAM generally captures the band of high tropospheric O_3 columns over West China.

[27] Figure 8 shows the time series of the REAM-simulated tropospheric O_3 columns and surface O_3 concentrations caused by the transport of O_3 from East Asia, South/central Asia, and the stratosphere at the WLG station and over West China from May to August in 2006. In terms of tropospheric columns, O_3 transported from the stratosphere is the dominant source both at the WLG station and over West China. The contribution by O_3 transported from East Asia is lower than that from South/central Asia over West China but comparable at the WLG station because the WLG station is closer to the polluted regions of East China. O_3 transported from South/central Asia increases from May to August because of the northward migration of the India summer monsoon. In terms of surface O_3 concentrations, the three factors are comparable at the WLG station and over West China. However, the summertime peaks of the surface O_3 concentrations at the WLG station reflect mainly the transport of O_3 from polluted regions nearby.

5. Conclusions

[28] Tropospheric O_3 columns retrieved from OMI and MLS measurements, CO columns retrieved from MOPITT, and lower tropospheric O_3 and CO concentrations retrieved from TES from May to August in 2006 are analyzed using

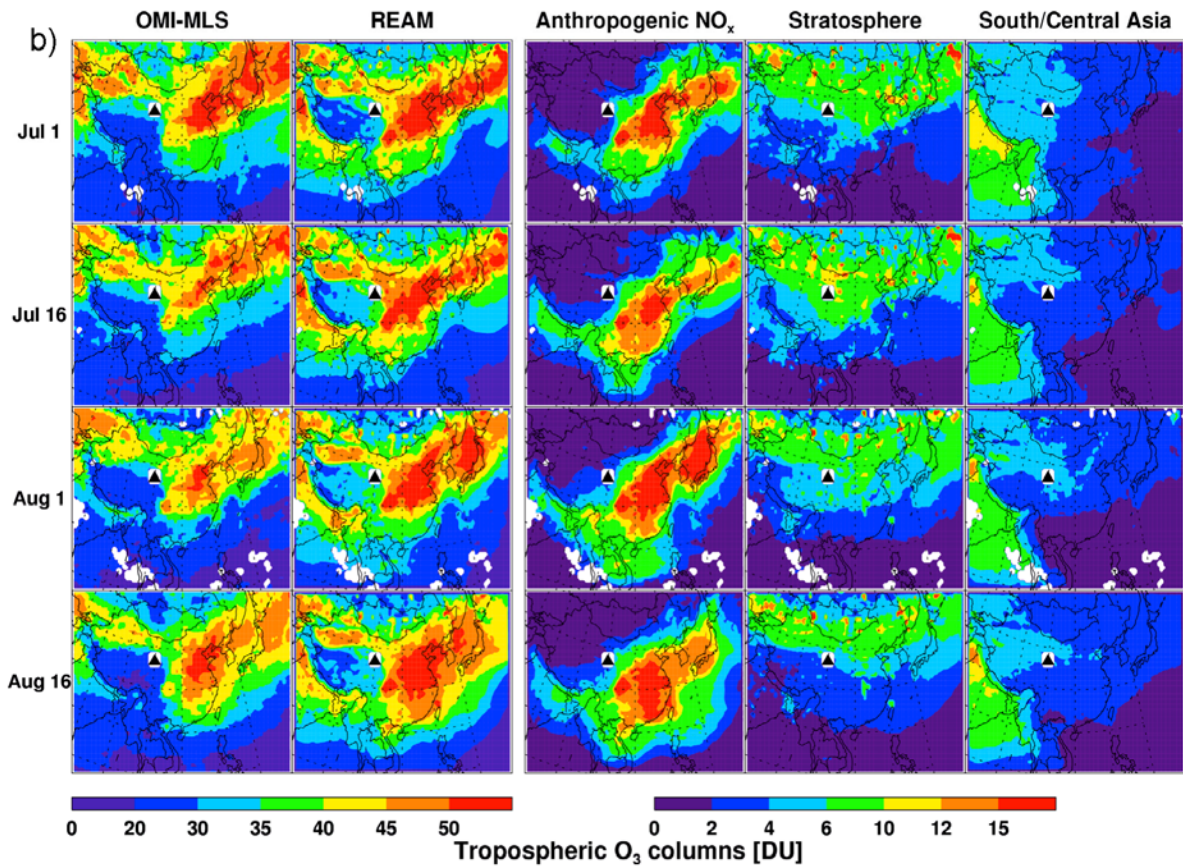


Figure 7. (continued)

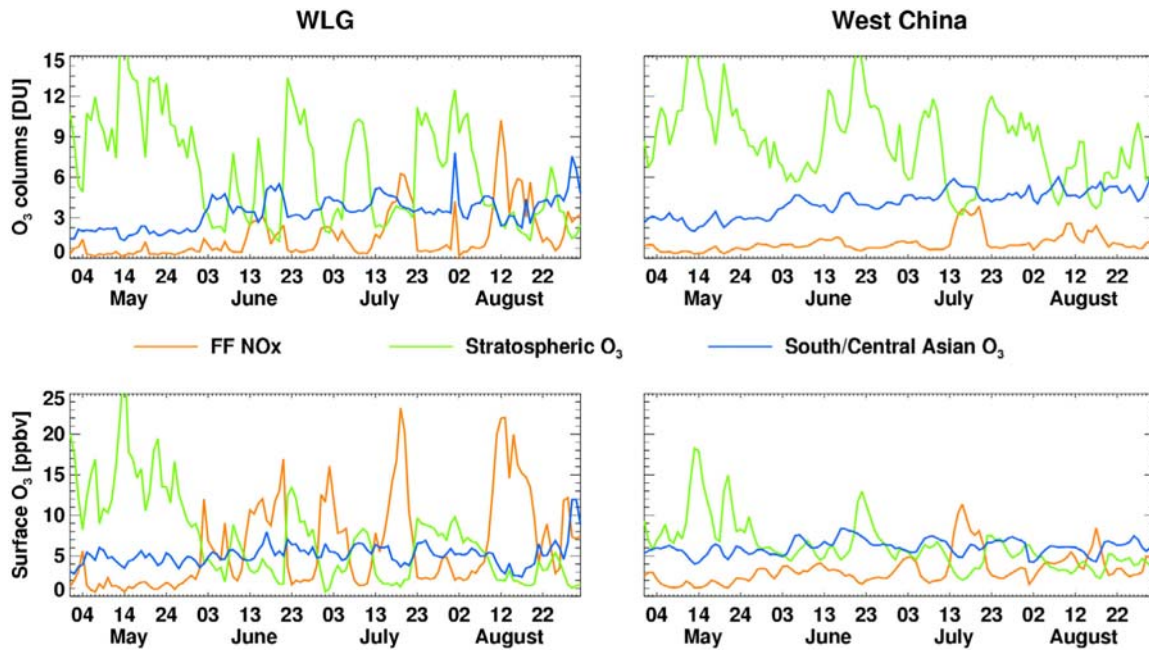


Figure 8. Time series of REAM-simulated contributions from anthropogenic NO_x emissions over East Asia (orange line), stratospheric transport (green line), and transport from South/central Asia (blue line) to daytime tropospheric O₃ columns (top) and surface O₃ (bottom) for May–August 2006 at the WLG station and over West China (36°N–42°N, 80°E–100°E).

REAM to investigate the spatially temporally resolved impact of the East Asian summer monsoon on the air quality over East China, a region with a concentrated pollutant source that hosts a major portion of the Chinese population. The large perturbation of air pollutant distributions over China by the onset and progress of East Asian summer monsoon is observed by satellites and simulated by REAM. Over monsoon-affected areas, ventilation by convection is faster, and the lower tropospheric photochemical processing is slower. Both MOPITT and TES measurements and REAM simulations show that CO enhancements over East China disappear with the onset of the monsoon and reemerge afterward. The monsoon impact is more significant on the CO concentrations in the lower troposphere than in the free troposphere.

[29] Both the TES 825 hPa O₃ concentrations and OMI-MLS tropospheric O₃ columns show a monsoon-driven bimodal distribution of tropospheric O₃ concentrations: high O₃ in the premonsoon period, rapid decrease in O₃ during monsoon, and O₃ recovery after monsoon. The analysis of the corresponding REAM simulations shows that the premonsoon tropospheric O₃ enhancement over East China is attributed to the combination of regional fast photochemical O₃ production and stratospheric transport. The monsoon season tropospheric O₃ minimum over East China results from the incursion of monsoonal inflow, which transports oceanic air masses with low O₃ concentrations. The moist air masses lead to convective ventilation and formation of clouds, which slows down the lower tropospheric photochemical process. The O₃ enhancement reemerges after mid-August when monsoon dissipates. While the summertime enhancements of tropospheric O₃ columns over West China and the WLG site are dominated by the stratospheric O₃ transport, surface O₃ over West China is modified by the O₃ transported from polluted East Asia and South/central Asia and the stratosphere.

[30] In this study, the independent satellite observations show consistent monsoon-associated perturbations of pollutant distributions. Satellite observations are capable of capturing the monsoon-associated variations of the lower tropospheric O₃ and CO and provide a precious opportunity to investigate the monsoon impact on the air quality over the monsoon regions of the globe, particularly those with relatively sparse surface measurements. Compared to the surface measurements, satellite observations provide a more detailed description of the monsoon impact on the distribution of tropospheric pollutants in terms of geographic features, which enables us to better understand the monsoon impact at a regional scale. While demonstrating the large-scale features of monsoon impact in the troposphere, a general lack of high-quality satellite observations near the surface is a major limitation for understanding the monsoon impact on surface air quality. Compared to the polar-orbiting satellite data used in this study, geostationary satellites would improve greatly the temporal resolution as well as the quality of time-averaged measurements.

[31] We find that the monsoon system strongly modulates the pollution problem over a large portion of heavily polluted East China in summer, depending on its strength and tempo-spatial extension. Xu et al. [2006], based on long-term surface wind measurements, suggested that pollutants over China have already caused a regional climate change, which sig-

nificantly weakens the East Asian summer monsoon circulation. Our results indicate that air quality of China in summer, in turn, will be vulnerable to the weakening of the monsoon circulation. Long-term satellite observations can potentially help us understand the response of air quality to variations of monsoon strength and tempo-spatial extension at a regional scale.

[32] **Acknowledgments.** This work was supported by the National Science Foundation Atmospheric Chemistry Program and the NASA Atmospheric Chemistry Modeling and Analysis Program. The GEOS-CHEM model is managed at Harvard University with support from the NASA Atmospheric Chemistry Modeling and Analysis Program.

References

- Beer, R. (2006), TES on the Aura mission: Scientific objectives, measurements and analysis overview, *IEEE Trans. Geosci. Remote Sens.*, *44*, 1102–1105, doi:10.1109/TGRS.2005.863716.
- Beer, R., T. A. Gilbavich, and D. M. Rider (2001), Tropospheric emission spectrometer for the Earth Observing System's Aura satellite, *Appl. Opt.*, *40*, 2356–2367, doi:10.1364/AO.40.002356.
- Bey, I., D. J. Jacob, R. M. Yantosca, J. A. Logan, B. D. Field, A. M. Fiore, Q. Li, H. Liu, L. J. Mickley, and M. G. Schultz (2001), Global modeling of tropospheric chemistry with assimilated meteorology: Model description and evaluation, *J. Geophys. Res.*, *106*, 23,073–23,096, doi:10.1029/2001JD000807.
- Choi, Y., Y. Wang, T. Zeng, R. V. Martin, T. P. Kurosu, and K. Chance (2005), Evidence of lightning NO_x and convective transport of pollutants in satellite observations over North America, *Geophys. Res. Lett.*, *32*, L02805, doi:10.1029/2004GL021436.
- Choi, Y., Y. Wang, T. Zeng, D. Cunnold, E. Yang, R. Martin, K. Chance, V. Thouret, and E. Edgerton (2008a), Springtime transitions of NO₂, CO, and O₃ over North America: Model evaluation and analysis, *J. Geophys. Res.*, *113*, D20311, doi:10.1029/2007JD009632.
- Choi, Y., Y. Wang, Q. Yang, D. Cunnold, T. Zeng, C. Shim, M. Luo, A. Eldering, E. Bucsela, and J. Gleason (2008b), Spring to summer northward migration of high O₃ over the western North Atlantic, *Geophys. Res. Lett.*, *35*, L04818, doi:10.1029/2007GL032276.
- Clerbaux, C., D. P. Edwards, M. Deeter, L. Emmons, J. Lamarque, X. Tie, S. Massie, and J. Gille (2008), Carbon monoxide pollution from cities and urban areas observed by the Terra/MOPITT mission, *Geophys. Res. Lett.*, *35*, L03817, doi:10.1029/2007GL032300.
- Deeter, M., et al. (2003), Operational carbon monoxide retrieval algorithm and selected results for the MOPITT instrument, *J. Geophys. Res.*, *108*(D14), 4399, doi:10.1029/2002JD003186.
- Deeter, M. N., D. P. Edwards, J. C. Gille, and J. R. Drummond (2007), Sensitivity of MOPITT observations to carbon monoxide in the lower troposphere, *J. Geophys. Res.*, *112*, D24306, doi:10.1029/2007JD008929.
- Ding, A., and T. Wang (2006), Influence of stratosphere-to-troposphere exchange on the seasonal cycle of surface ozone at Mount Waliguan, western China, *Geophys. Res. Lett.*, *33*, L03803, doi:10.1029/2005GL024760.
- Ding, Y., and J. Chan (2005), The East Asian summer monsoon: An overview, *Meteorol. Atmos. Phys.*, *89*, 117–142, doi:10.1007/s00703-005-0125-z.
- Emmons, L., D. Edwards, M. Deeter, J. Gille, T. Campos, P. Nedelec, P. Novelli, and G. Sachse (2009), Measurements of pollution in the troposphere (MOPITT) validation through 2006, *Atmos. Chem. Phys.*, *9*, 1795–1803.
- Fu, R., Y. Hu, J. Wright, J. Jiang, R. Dickinson, M. Chen, M. Filipiak, W. Read, J. Waters, and D. Wu (2006), Short circuit of water vapor and polluted air to the global stratosphere by convective transport over the Tibetan Plateau, *Proc. Natl. Acad. Sci. U. S. A.*, *103*, 5664–5669.
- Guillas, S., J. Bao, Y. Choi, Y. Wang, H. Khaing, C. Nesbit, and G. Huey (2008), Downscaling of chemical transport ozone forecasts over Atlanta, *Atmos. Environ.*, *42*, 1338–1348, doi:10.1016/j.atmosenv.2007.10.027.
- Halland, J., H. Fuelberg, K. Pickering, and M. Luo (2009), Identifying convective transport of carbon monoxide by comparing remotely sensed observations from TES with cloud modeling simulations, *Atmos. Chem. Phys.*, *9*, 4279–4294.
- He, Y., I. Uno, Z. Wang, P. Pchanart, J. Li, and H. Akimoto (2008), Significant impact of the East Asia monsoon on ozone seasonal behavior in the boundary layer of Eastern China and the west Pacific region, *Atmos. Chem. Phys.*, *8*, 7543–7555.

- Hoskins, B. J., and M. J. Rodwell (1995), A model of the Asian summer monsoon I. The global scale, *J. Atmos. Sci.*, *52*, 1329–1340, doi:10.1175/1520-0469(1995)052<1329:AMOTAS>2.0.CO;2.
- Huang, G. (2004), An index measuring the interannual variation of the East Asian summer monsoon—The EAP index, *Adv. Atmos. Sci.*, *21*, 41–52, doi:10.1007/BF02915679.
- Huffman, G. J., R. F. Adler, M. Morrissey, D. T. Bolvin, S. Curtis, R. Joyce, B. McGavock, and J. Susskind (2001), Global precipitation at one-degree daily resolution from multi-satellite observations, *J. Hydrometeorol.*, *2*, 36–50, doi:10.1175/1525-7541(2001)002<0036:GPAODD>2.0.CO;2.
- Jiang, J., N. Livesey, H. Su, L. Neary, J. McConnell, and N. Richards (2007), Connecting surface emissions, convective uplifting, and long-range transport of carbon monoxide in the upper troposphere: New observations from the Aura Microwave Limb Sounder, *Geophys. Res. Lett.*, *34*, L18812, doi:10.1029/2007GL030638.
- Jing, P., D. Cunnold, Y. Choi, and Y. Wang (2006), Summertime tropospheric ozone columns from Aura OMI/MLS measurements versus regional model results over the United States, *Geophys. Res. Lett.*, *33*, L17817, doi:10.1029/2006GL026473.
- Jones, D. B. A., K. W. Bowman, P. I. Palmer, J. Worden, D. Jacob, R. Hoffman, I. Bey, and R. Yantosca (2003), Potential of observations from the Tropospheric Emission Spectrometer to continental sources of carbon monoxide, *J. Geophys. Res.*, *108*(D24), 4789, doi:10.1029/2003JD003702.
- Jourdain, L., et al. (2007), Tropospheric vertical distribution of tropical Atlantic ozone observed by TES during the northern African biomass burning season, *Geophys. Res. Lett.*, *34*, L04810, doi:10.1029/2006GL028284.
- Kar, J., et al. (2008), Measurement of low-altitude CO over the Indian subcontinent by MOPITT, *J. Geophys. Res.*, *113*, D16307, doi:10.1029/2007JD009362.
- Li, J., and Q. Zeng (2002), A unified monsoon index, *Geophys. Res. Lett.*, *29*(8), 1274, doi:10.1029/2001GL013874.
- Li, J., Z. Wang, H. Akimoto, C. Gao, P. Pochanart, and X. Wang (2007), Modeling study of ozone seasonal cycle in lower troposphere over East Asia, *J. Geophys. Res.*, *112*, D22S25, doi:10.1029/2006JD008209.
- Ma, J., H. Liu, and D. Hauglustaine (2002), Summertime tropospheric ozone over China simulated with a regional chemical transport model: 1. Model description and evaluation, *J. Geophys. Res.*, *107*(D22), 4660, doi:10.1029/2001JD001354.
- Park, M., W. Randel, A. Gettelman, S. Massie, and J. Jiang (2007), Transport above the Asian summer monsoon anticyclone inferred from Aura Microwave Limb Sounder tracers, *J. Geophys. Res.*, *112*, D16309, doi:10.1029/2006JD008294.
- Randel, W., and M. Park (2006), Deep convective influence on the Asian summer monsoon anticyclone and associated tracer variability observed with Atmospheric Infrared Sounder (AIRS), *J. Geophys. Res.*, *111*, D12314, doi:10.1029/2005JD006490.
- Richter, A., J. P. Burrows, H. Nub, C. Granier, and U. Niemeier (2005), Increase in tropospheric nitrogen dioxide over China observed from space, *Nature*, *437*, 129–132, doi:10.1038/nature04092.
- Rodwell, M. J., and B. J. Hoskins (2001), Subtropical anticyclones and summer monsoons, *J. Clim.*, *14*, 3192–3211, doi:10.1175/1520-0442(2001)014<3192:SAASM>2.0.CO;2.
- Shim, C., et al. (2009), Satellite observation of Mexico City pollution outflow from the Tropospheric Emissions Spectrometer (TES), *Atmos. Environ.*, *43*, 1540–1547, doi:10.1016/j.atmosenv.2008.11.026.
- Streets, D. G., and S. T. Waldhoff (2000), Present and future emissions of air pollutants in China: SO₂, NO_x, and CO, *Atmos. Environ.*, *34*, 363–374, doi:10.1016/S1352-2310(99)00167-3.
- Streets, D. G., et al. (2003), An inventory of gaseous and primary aerosol emissions in Asia in the year 2000, *J. Geophys. Res.*, *108*(D21), 8809, doi:10.1029/2002JD003093.
- Tanimoto, H., Y. Sawa, H. Matsueda, I. Uno, T. Ohara, K. Yamaji, J. Kurokawa, and S. Yonemura (2005), Significant latitudinal gradient in the surface ozone spring maximum over East Asia, *Geophys. Res. Lett.*, *32*, L21805, doi:10.1029/2005GL023514.
- Wang, B., and H. Lin (2002), Rainy season of the Asian-Pacific summer monsoon, *J. Clim.*, *15*, 386–396, doi:10.1175/1520-0442(2002)015<0386:RSOTAP>2.0.CO;2.
- Wang, H., L. Zhou, and X. Tang (2006), Ozone concentrations in rural regions of the Yangtze Delta in China, *J. Atmos. Chem.*, *54*, 255–265, doi:10.1007/s10874-006-9024-z.
- Wang, T., H. Wong, J. Tang, A. Ding, W. Wu, and X. Zhang (2006), On the origin of surface ozone and reactive nitrogen observed at a remote mountain site in the northeastern Qinghai-Tibetan Plateau, western China, *J. Geophys. Res.*, *111*, D08303, doi:10.1029/2005JD006527.
- Wang, Y., D. J. Jacob, and J. A. Logan (1998), Global simulation of tropospheric O₃-NO_x-hydrocarbon chemistry: 1. Formulation, *J. Geophys. Res.*, *103*, 10,713–10,725, doi:10.1029/98JD00158.
- Wang, Y., Y. Choi, T. Zeng, B. Ridley, N. Blake, D. Blake, and F. Flocke (2006), Late-spring increase of trans-Pacific pollution transport in the upper troposphere, *Geophys. Res. Lett.*, *33*, L01811, doi:10.1029/2005GL024975.
- Wang, Y., Y. Choi, T. Zeng, D. Davis, M. Bühr, G. Huey, and W. Neff (2007), Assessing the photochemical impact of snow NO_x emissions over Antarctica during ANTCTI 2003, *Atmos. Environ.*, *41*, 3944–3958, doi:10.1016/j.atmosenv.2007.01.056.
- Wang, Z., J. Li, X. Wang, P. Pochanart, and H. Akimoto (2006), Modeling of regional high ozone episode observed at two mountain sites (Mt. Tai and Huang) in East China, *J. Atmos. Chem.*, *55*, 253–272, doi:10.1007/s10874-006-9038-6.
- Wei, F., E. Teng, G. Wu, W. Hu, W. Wilson, R. Chapman, J. Pau, and J. Zhang (1999), Ambient concentrations and elemental compositions of PM₁₀ and PM_{2.5} in four Chinese cities, *Environ. Sci. Technol.*, *33*(23), 4188–4193, doi:10.1021/es9904944.
- Worden, H., et al. (2007), Comparisons of Tropospheric Emission Spectrometer (TES) ozone profiles to ozonesondes: Methods and initial results, *J. Geophys. Res.*, *112*, D03309, doi:10.1029/2006JD007258.
- Worden, J., et al. (2009), Observed vertical distribution of tropospheric ozone during the Asian summertime monsoon, *J. Geophys. Res.*, *114*, D13304, doi:10.1029/2008JD010560.
- Xu, M., C.-P. Chang, C. Fu, Y. Qi, A. Robock, D. Robinson, and H. Zhang (2006), Steady decline of east Asian monsoon winds, 1969–2000: Evidence from direct ground measurements of wind speed, *J. Geophys. Res.*, *111*, D24111, doi:10.1029/2006JD007337.
- Yang, Q., D. Cunnold, H. Wang, L. Froidevaux, H. Claude, J. Merrill, M. Newchurch, and S. Oltmans (2007), Midlatitude tropospheric ozone columns derived from the Aura Ozone Monitoring Instrument and Microwave Limb Sounder measurements, *J. Geophys. Res.*, *112*, D20305, doi:10.1029/2007JD008528.
- Yang, Q., D. M. Cunnold, Y. Choi, Y. Wang, J. Nam, H.-J. Wang, L. Froidevaux, A. M. Thompson, and P. K. Bhartia (2009), A study of tropospheric ozone column enhancements over North America using satellite data and a global chemical model, *J. Geophys. Res.*, doi:10.1029/2009JD012616, in press.
- Zeng, T., Y. Wang, K. Chance, E. V. Browell, B. A. Ridley, and E. L. Atlas (2003), Widespread persistent near-surface ozone depletion at northern high latitudes in spring, *Geophys. Res. Lett.*, *30*(24), 2298, doi:10.1029/2003GL018587.
- Zeng, T., Y. Wang, K. Chance, N. Blake, D. Blake, and B. Ridley (2006), Halogen-driven low altitude O₃ and hydrocarbon losses in spring at northern high latitudes, *J. Geophys. Res.*, *111*, D17133, doi:10.1029/2005JD006706.
- Zhang, L., et al. (2006), Ozone-CO correlations determined by the TES satellite instrument in continental outflow regions, *Geophys. Res. Lett.*, *33*, L18804, doi:10.1029/2006GL026399.
- Zhang, Q., et al. (2009), Asian emissions in 2006 for the NASA INTEX-B mission, *Atmos. Chem. Phys.*, *9*, 5131–5153.
- Zhang, Z., J. Chan, and Y. Ding (2004), Characteristics, evolution and mechanisms of the summer monsoon onset over Southeast Asia, *Int. J. Climatol.*, *24*, 1461–1482, doi:10.1002/joc.1082.
- Zhao, C., and Y. Wang (2009), Assimilated inversion of NO_x emissions over East Asia using OMI NO₂ column measurements, *Geophys. Res. Lett.*, *36*, L06805, doi:10.1029/2008GL037123.
- Zhao, C., Y. Wang, and T. Zeng (2009a), East China plains: A “basin” of ozone pollution, *Environ. Sci. Technol.*, *43*, 1911–1915, doi:10.1021/es8027764.
- Zhao, C., Y. Wang, Y. Choi, and T. Zeng (2009b), Summertime impact of convective transport and lightning NO_x production over North America: Modeling dependence on meteorological simulations, *Atmos. Chem. Phys.*, *9*, 4315–4327.
- Zhu, B., H. Akimoto, Z. Wang, K. Sudo, J. Tang, and I. Uno (2004), Why does surface ozone peak in summertime at Waliguan?, *Geophys. Res. Lett.*, *31*, L17104, doi:10.1029/2004GL020609.

Y. Choi, Jet Propulsion Laboratory, California Institute of Technology, Pasadena, CA 91109, USA.

R. Fu, Jackson School of Geosciences, The University of Texas at Austin, Austin, TX 78712, USA.

Y. Wang and Q. Yang, School of Earth and Atmospheric Sciences, Georgia Institute of Technology, Atlanta, GA 30332, USA.

C. Zhao, Atmospheric Sciences and Global Change Division, Pacific Northwest National Laboratory, Richland, WA 99354, USA. (chun.zhao@pnl.gov)